

Multiscale Modeling of Materials - Concepts and Illustration

Aditi Mallik, Keith Runge, James W. Dufty, and Hai-Ping Cheng

Department of Physics, University of Florida, Gainesville, FL 32611

(Dated: January 25, 2022)

Abstract

The approximate representation of a quantum solid as an equivalent composite semi-classical solid is considered for insulating materials. The composite is comprised of point ions moving on a potential energy surface. In the classical bulk domain this potential energy is represented by pair potentials constructed to give the same structure and elastic properties as the underlying quantum solid. In a small local quantum domain the potential is determined from a detailed quantum calculation of the electronic structure. The formulation of this description as a sequence of physical approximations is considered in some detail. The primary new ingredients are 1) a determination of the pair potential from quantum chemical data for equilibrium and strained structures, 2) development of 'pseudo-atoms' for a realistic treatment of charge densities where bonds have been broken to define the quantum domain, and 3) inclusion of polarization effects on the quantum domain due to its environment. This formal structure is illustrated in detail for an SiO_2 nanorod. For each configuration considered, the charge density of the entire solid is calculated quantum mechanically to provide the reference by which to judge the accuracy of the modeling. The construction of the pair potential, the rod, the pseudo-atoms, and the multipoles is discussed and tested in detail. It is then shown that the quantum rod, the rod constructed from the classical pair potentials, and the composite classical/quantum rod all have the same equilibrium structure and response to elastic strain. In more detail, the charge density and forces in the quantum subdomain are accurately reproduced by the proposed modeling of the environmental effects even for strains beyond the linear domain. The accuracy of the modeling is shown to apply for two quite different quantum chemical methods for the underlying quantum mechanics: transfer Hamiltonian and density functional methods.

I. INTRODUCTION

The field of multiscale modeling has opened a new era to computational science for studying complex phenomena like fracture, hydrolysis, enzymatic reactions, solute-solvent studies, hydrogen embrittlement, and many other chemo-mechanical processes in macroscopic samples. Often these phenomena require a very accurate description at one scale, while at another scale a much coarser method can be applied to get satisfactory results. In fact, the coarser description for the bulk sample is required because the more fundamental methods are computationally too intensive to be applied to the entire system. These scales may be length or time, or a combination of both. This scheme of combining different models at different scales to achieve a balance of accuracy, efficiency, and realistic description is known as multiscale modeling. It is accomplished by applying the high accuracy method only in a small domain where it is needed the most and more approximate methods for the rest of the bulk where they are appropriate. For example, in crack propagation one has to apply detailed quantum mechanics at the tip of the crack. Here the bonds are breaking between the atoms, causing a marked deformation of the electron cloud and charge transfer between ions. But far from the crack tip where the atoms are less deformed they can be described by classical mechanics with appropriate potentials. Thus, the problem arises of linking quite different descriptions for the different length scales¹.

There is a broad diversity of other examples requiring multiscale modeling: chemo-mechanical polishing², tidal wave prediction³, atmospheric sciences, embrittlement of nuclear reactors⁴, and many biological systems⁵. Two classes can be distinguished⁶, “serial multiscale modeling” where the various scales are weakly coupled but the computation of parameters at smaller scales is required for its use in more phenomenological models at a larger scale, and “concurrent multiscale modeling” where the various descriptions applied on different scales should all be nested with proper boundary conditions. The multiscale modeling discussed here is of the “concurrent” type, although there are components that can be considered as the “serial” type (e.g., parameterization of the underlying approximate quantum method used).

Three different length scale levels are distinguished, the nanoscale where the details of electron structure and quantum chemistry are important, the atomic or microscale where appropriate classical pair potentials capture the structure accurately, and the macroscale where

a continuum mechanical description applies. The present work addresses only one particular subclass of multiscale modeling, known as hybrid quantum mechanical (QM)/classical mechanical (CM) problems, and their application to solid insulators - silica in particular. The further embedding of the atomic scale in a macroscale model is not considered here. Early work on this QM/CM topic began with Warshel and Levitt⁷ and has accelerated over the past decade⁸. Applications of QM/CM include biological systems where this scheme is sometimes referred to as QM/MM (molecular mechanics) modeling (enzymes, DNAs and proteins)^{9,10,11,12,13}, vibrational spectroscopy¹⁴, electronic excitations^{8,15,16}, hydrolysis of silica^{17,18}, and solute-solvent problems^{19,20,21}.

The challenge of the QM/CM simulation is to move from one length scale to another, as smoothly as possible. A solid or large cluster behaves as a single "molecule" so the partitioning becomes more complicated due to covalent bonds that are cut between the QM and CM regions. These dangling bonds give rise to incorrect charge densities in the QM domain and other pathologies^{22,23}. A multiscale modeling scheme is proposed here that addresses this and other problems of the quantum embedding to provide a means for faithful coupling between the QM and CM regions. There are many tests for fidelity across the QM/CM interface, such as bond angles, bond lengths, and proton affinities. Instead, the criteria here are preservation of accurate electronic charge densities and total forces in the QM sub domain. These are the physically significant properties based more closely in the theoretical structure being modeled, as described in the next section. The approach includes the following two components:

- (i) Modeling environmental effects for the quantum domain in an accurate and simple manner. Here, accurate means that the forces and charge densities of the QM domain are reproduced to within a few percent. This entails a chemically correct treatment of the dangling bonds, and an account of longer range Coulomb influences from the classical domain. Simplicity, means that the approximations made are transparent and that the difficulty of the quantum calculation is not increased. Here, the valency problem is solved by pseudo-atoms and the longer range environmental effects are included through low order polarization effects²⁴.

- (ii) Developing a new classical potential for the classical region tailored to the properties of interest. A new potential for the entire CM region is designed, based on selected force data calculated from the quantum method used in the QM domain. This data is generated for

both equilibrium and near equilibrium states. The test for a suitable potential, in addition to producing the right structure, is the accurate reproduction of the chosen property to be studied, for near equilibrium states (typically some linear response characteristic)²⁵. The use of this new potential prevents any mismatch of that response property across the QM/CM boundary. Hence different problems (fracture or corrosion) might require the construction of different potentials for the same system.

The criterion for the success of (i) and (ii) is that calculations of the desired properties should be indistinguishable for the quantum system, purely classical system, and the composite QM/CM system for near equilibrium states. Only then are the desired applications to far from equilibrium states reliable.

In the next four sections, the theoretical basis for this modeling scheme is described in some detail. The object is to provide a means to assess the approximations made more directly, and also to provide the basis for their extension to other systems. The complete formalism is then tested for a model system - a silica nanorod²⁶ (Figure 1) - in section VI. This silica nanorod containing 108 nuclei has been chosen since a quantum treatment of the whole sample is possible to assess quantitatively all aspects of the proposed scheme. Still, the system is big enough to yield bulk properties like stress-strain response (also shown in Figure 1). The nanorod has the proper stoichiometric ratio of silicon to oxygen observed in real silica (1:2) and is considered a viable model for studying silica. One of the rings near the center of the rod is chosen to be the QM domain and rest of the rod is treated classically (see Figure 6 below).

The system is studied under uniaxial strain. The quantum mechanical method used is the Transfer Hamiltonian (TH) method²⁷ using an NDDO type theory parameterized by coupled cluster data (described more completely in section VI). The construction of the classical pair potential is described and shown to yield the same Young's constant as obtained from the QM calculation, to within a few percent. Next, the training of the pseudo atoms and validity of polarization representation for the environment of the QM system is tested. The resulting force and charge densities for the QM domain are accurately reproduced to within a few percent. Finally, the composite QM/CM rod is shown to have the same structure and elastic properties as both the QM and CM rods for near equilibrium states, as required. The entire analysis is repeated using density functional theory (DFT) as the underlying quantum theory, instead of the TH quantum mechanics. The same level of accuracy for the modeling

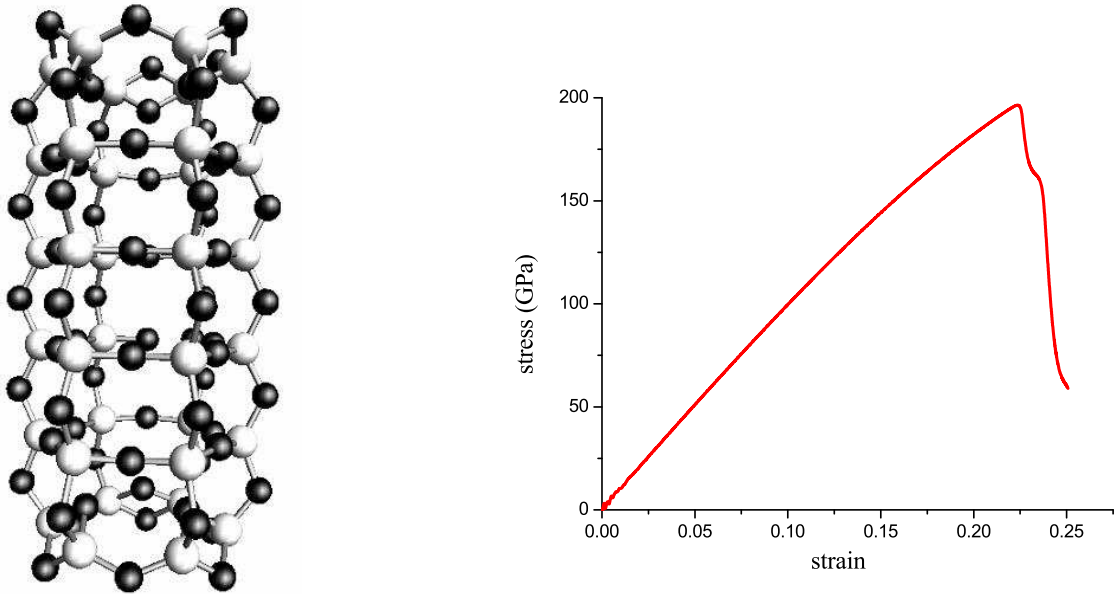


FIG. 1: (color online) Structure of the SiO_2 nanorod (left), and quantum stress - strain curve showing bulk solid properties (right)

is found to hold in this case as well.

II. THE IDEALIZED QUANTUM SOLID

In this section the problem of multiscale modeling is introduced by first stating clearly what is the system being modeled. While much of this introductory matter is familiar, it provides the context for assessing *all* approximations involved in the final model material. First, the quantum description in terms of ions and electrons is given and the limitations for practical implementation are noted. Next, reduced self-consistent descriptions are given for the ions and electrons, each coupled to the other through their average charge density. In this form the classical limit for the ions can be taken, allowing the use of MD simulation methods for their dynamics. The equation for the electrons is simplified in a different direction, exploiting the very different time scales for electron and nuclear motion (the Born-Oppenheimer limit). This final description constitutes the idealized quantum solid for which the subsequent multiscale modeling scheme is proposed.

At the fundamental level a simple atomic or molecular solid can be described in terms of N_i "ions" with charge number Z_i for the corresponding atoms of species i and a set of

N_e electrons, with overall charge neutrality ($\sum_i N_i Z_i = N_e$). To introduce the various levels of description it is useful to start with the density operator D for the system as a whole. Properties of interest A are given by the expectation value

$$\langle A \rangle = \text{Tr}_{e,i} D A, \quad (1)$$

where the trace is taken over all electron and ion degrees of freedom. The density operator obeys the Liouville - von Neumann equation

$$\partial_t D + \frac{i}{\hbar} [H, D] = 0. \quad (2)$$

The Hamiltonian operator H is comprised of the Hamiltonians H_i and H_e for the isolated systems of ions and electrons, respectively, and their interaction U_{ie}

$$H = H_i + H_e + U_{ie}, \quad (3)$$

$$U_{ie} = \int d\mathbf{r} d\mathbf{r}' \frac{\rho_i(\mathbf{r}) \rho_e(\mathbf{r}')}{|\mathbf{r} - \mathbf{r}'|}. \quad (4)$$

Here $\rho_i(\mathbf{r})$ and $\rho_e(\mathbf{r})$ are the ion and electron charge density operators. This is the most fundamental level for a quantum description of the system. For a pure state, D is a projection onto a state Ψ which is determined from the corresponding Schroedinger equation. For small systems, this can be solved numerically by quantum Monte Carlo methods. At this level, the approximations involved (e.g., electron nodal location) can be considered mild and under control. However, quantum Monte Carlo methods are restricted to relatively small systems and the above fundamental description is not a practical method for application to larger systems, particularly if repeated calculation is required to follow the dynamics.

In many cases the properties of interest are functions only of the ion degrees of freedom (e.g. structure), $A \rightarrow A_i$, or they are purely electronic (e.g., optical), $A \rightarrow A_e$. Then a description is possible in terms the reduced density operators for the ions and for the electrons, D_i and D_e , resulting from appropriate partial traces over all the electrons or ions, respectively

$$\langle A_i \rangle = \text{Tr}_i D_i A_i, \quad \langle A_e \rangle = \text{Tr}_e D_e A_e, \quad (5)$$

$$D_i \equiv \text{Tr}_e D, \quad D_e \equiv \text{Tr}_i D. \quad (6)$$

Their equations follow directly from (2)

$$\partial_t D_i + \frac{i}{\hbar} [H_i, D_i] + \frac{i}{\hbar} (U_i D_i - D_i U_i^\dagger) = 0, \quad (7)$$

$$\partial_t D_e + \frac{i}{\hbar} [H_e, D_e] + \frac{i}{\hbar} (U_e D_e - D_e U_e^\dagger) = 0. \quad (8)$$

where the potential energy operators coupling the ion and electronic degrees of freedom are

$$U_i = \int d\mathbf{r} d\mathbf{r}' \frac{1}{|\mathbf{r} - \mathbf{r}'|} \rho_i(\mathbf{r}) \tilde{\rho}_e(\mathbf{r}'), \quad \tilde{\rho}_e(\mathbf{r}) = (Tr_e \rho_e(\mathbf{r}) D) (Tr_e D)^{-1}, \quad (9)$$

$$U_e = \int d\mathbf{r} d\mathbf{r}' \frac{1}{|\mathbf{r} - \mathbf{r}'|} \tilde{\rho}_i(\mathbf{r}) \rho_e(\mathbf{r}'), \quad \tilde{\rho}_i(\mathbf{r}) = (Tr_i \rho_i(\mathbf{r}) D) (Tr_i D)^{-1} \quad (10)$$

This is similar to the microscopic ion - electron coupling of (4) except that now the electron charge density operator $\rho_e(\mathbf{r})$ is replaced by its conditional average, $\tilde{\rho}_e(\mathbf{r})$, in the equation for D_i , and the ion charge density $\rho_i(\mathbf{r})$ is replaced by its conditional average, $\tilde{\rho}_i(\mathbf{r})$ in the equation for D_e . The description (7) and (8) is still exact but formal since these average charge densities are not determined by these equations alone. The simplest realistic approximation (mean field) is to neglect the direct correlations in the charge densities $\tilde{\rho}_i(\mathbf{r})$ and $\tilde{\rho}_e(\mathbf{r})$, i.e. replace $D \rightarrow D_e D_i$ in (7) and (10) to get

$$\tilde{\rho}_i(\mathbf{r}) \rightarrow Tr_i \rho_i(\mathbf{r}) D_i \equiv \bar{\rho}_i(\mathbf{r}), \quad \tilde{\rho}_e(\mathbf{r}) \rightarrow Tr_e \rho_e(\mathbf{r}) D_e \equiv \bar{\rho}_e(\mathbf{r}). \quad (11)$$

As a consequence, the potentials U_i and U_e become Hermitian and the average charge densities are now self-consistently determined by (7) and (8). Self-consistency is required since D_e and D_i are functionals of the average charge densities $\bar{\rho}_i(\mathbf{r})$ and $\bar{\rho}_e(\mathbf{r})$, respectively.

The advantage of this reduced description is that the ions and electrons are described by separate equations, reducing the degree of difficulty of each. More importantly, this separation allows the introduction of appropriate approximations for each. The large differences in electron and ion masses imply corresponding differences in time scales and thermal de Broglie wavelengths. Consequently, the equation for the ions admits a classical limit for the conditions of interest, while that for the electrons does not. The classical limit of equation (7) becomes

$$\partial_t D_i + \{(H_i + U_i[\bar{\rho}_e]), D_i\} = 0, \quad (12)$$

where $\{, \}$ now denotes a Poisson bracket operation, and D_i is a function of the ion positions and momenta, $D_i \rightarrow D_i(\{\mathbf{R}_{i\alpha}\}, \{\mathbf{P}_{i\alpha}\}, t)$ (here α denotes a specific ion). This equation now

can be solved accurately and efficiently by molecular dynamics simulation methods, even for large systems. This is an essential step in almost all practical descriptions of bulk materials whose importance cannot be overstated.

Implementation of (12) still requires calculation of the potential energy $U_i [\bar{\rho}_e]$, which in turn requires determination of the electronic charge density from D_e . However, the general solution to (8) is a formidable problem: determination of the dynamics of N_e electrons self-consistently in the presence of a changing ion charge density. Two simplifications are made to bring this problem under control. First, it is recognized that $\tau (\partial_t D_i) D_i^{-1} \ll 1$, where τ is the time scale for changes in the electron distribution function D_e . Second, it is assumed that only the lowest energy state contributes to D_e at any given time. The first approximation constitutes the Born-Oppenheimer approximation while the second approximation is appropriate for most structural studies, but must be relaxed for optical studies involving electronic transitions. In principle, (12) is solved in time steps Δt . At each time step the electronic charge density is computed for the ion configurations at that time step in order to recompute new forces for the next time step. The electronic charge density calculation is a ground state eigenvalue problem for the given ion configuration.

To summarize, the final description of this idealized solid, it consists of a set of point ions governed by the classical equation (12) for their probability distribution $D_i \rightarrow D_i(\{\mathbf{R}_{i\alpha}\}, \{\mathbf{P}_{i\alpha}\}, t)$

$$\partial_t D_i + \{(H_i + U_i [\bar{\rho}_e]), D_i\} = 0, \quad (13)$$

$$U_i = \int d\mathbf{r} d\mathbf{r}' \frac{1}{|\mathbf{r} - \mathbf{r}'|} \rho_i(\mathbf{r}) \bar{\rho}_e(\mathbf{r}', t), \quad \bar{\rho}_e(\mathbf{r}, t) = Tr_e \rho_e(\mathbf{r}') D_e [\bar{\rho}_i] \quad (14)$$

The average electron density $\bar{\rho}_e(\mathbf{r})$ is determined from the ground state solution to (8)

$$\frac{i}{\hbar} [H_e + U_e, D_e] = 0, \quad (15)$$

$$U_e = \int d\mathbf{r} d\mathbf{r}' \frac{1}{|\mathbf{r} - \mathbf{r}'|} \bar{\rho}_i(\mathbf{r}, t) \rho_e(\mathbf{r}'), \quad \bar{\rho}_i(\mathbf{r}, t) = Tr_e \rho_i(\mathbf{r}) D_i [\bar{\rho}_e] \quad (16)$$

The analysis proceeds stepwise. The classical equations (13) are solved analytically in discrete time steps for the atomic coordinates and momenta. At each step the electron problem (15) is solved for the electron ground state using the ion configuration at the previous time step. From this ground state the electron charge density $\rho_e(\mathbf{r})$ is determined. This gives the potential energy function U_i and consequently the forces required to change the ion positions

and momenta at the next time step. The process is repeated with a new electron charge density calculated at each time step using the new ionic configurations. All electron correlations are accounted for quantum mechanically in the eigenvalue problem; all atomic correlations are determined classically through direct solution of Newton's equations. All structural properties of interest can be calculated since the phase points for the ions are known at all times. The dynamics of the electrons is only coarse-grained as they are "slaved" to the time dependence of the ions.

The above defines a "quantum molecular dynamics" representation of the idealized quantum solid. The semi-classical approximation for the ions, and ground state Born-Oppenheimer approximation for the electrons are relatively weak under most conditions of interest. The resulting description allows an accurate classical treatment of the ionic structure while retaining relevant quantum chemistry for the interatomic forces due to electrons. If it could be implemented in practice for bulk systems of interest over reasonable time intervals there would be little need for multiscale modeling. With MD simulation the solution to (13) once U_i has been provided is straightforward. So the problem has been reduced to a determination of the electron charge density. Unfortunately, the solution to (15) using realistic quantum chemical methods for even a few hundred ions at each time step becomes prohibitively time intensive.

III. THE FORMAL PARTITION AND COMPOSITE SOLID

A. The Representative Classical Solid

In many cases of interest (e.g., equilibrium structure, thermodynamics) the computational limitations of quantum chemical methods can be avoided through a purely classical representation of the solid, avoiding the intensive electron charge density calculation at each time step. This entails an idealization that has many variants. It consists of the representation of the true potential energy function $U_i(\{\mathbf{R}_{i\alpha}\})$ in (13) by a suitably *chosen* function $U_c(\{\mathbf{R}_{i\alpha}\})$. Consequently, its form does not need to be computed at each time step and the speed and efficiency of classical molecular dynamics is not compromised.

The problem with this approach lies in the choice for $U_c(\{\mathbf{R}_{i\alpha}\})$. In principle, an exact

mapping for some fundamental property such as the free energy F can be imposed

$$F[U_i] = F_c[U_c]. \quad (17)$$

where F_c is the corresponding classical functional. Generally, such exact methods can be inverted only perturbatively and lead to a sequence of effective many ion interactions involving increasingly more particles. A more practical method is to assume pairwise additivity for effective point "atoms"

$$U_c(\{\mathbf{R}_{i\alpha}\}) \rightarrow \frac{1}{2} \sum_{k,j} \sum_{\alpha}^{N_k} \sum_{\beta}^{N_j} V_{kj}(|\mathbf{R}_{k\alpha} - \mathbf{R}_{j\beta}|), \quad (18)$$

where k, i label the species (ion or electron). The exact determination of the pair potentials $V_{kj}(|\mathbf{R}_{k\alpha} - \mathbf{R}_{j\beta}|)$ is now much more restrictive as not all properties of interest have such a representation. Nevertheless pair properties such as the radial distribution functions $g_{kj}(|\mathbf{r}|)$ might be used to determine the pair potentials. As the $g_{kj}(|\mathbf{r}|)$ are unknown and difficult to calculate, the inversion is again difficult and not practical. Instead, experimental data is often used to fit a parameterized functional form chosen for the pair potentials. At this stage control over the approximation is lost and the method becomes phenomenological.

This phenomenological approach has been and remains a valuable tool of materials sciences. However, in the context of multiscale modeling it must be reconsidered carefully. First, it is recognized that there are local domains far from equilibrium where a purely classical potential cannot apply because of the inherent quantum chemistry active there (e.g., charge transfer and exchange). Conversely, there are large complementary domains in near equilibrium states where representation by an appropriate classical potential is possible. Multiscale modeling constructs distinct classical and quantum models of these subsystems and then requires fidelity at their interface. This is a severe test of the modeling assumptions in each subsystem. The approach proposed here confronts this issue directly in the construction of appropriate pair potentials for the problem considered.

B. The Composite Quantum/Classical Solid

It is presumed that there is some method for identifying domains within the solid for which quantum chemical effects should be treated in detail. The quantum solid is then represented as a composite of two domains, the larger bulk in which a classical representation is used

and a smaller "reactive" domain in which the original quantum description is retained. The objective of the modeling described here is therefore to construct the potential function U_i such that it gives an accurate description in both the reactive and non-reactive domains. This has two components, the determination of a pair potential for the forces on ions in the classical domain, and an accurate calculation of the charge density for the forces on ions in the quantum domain.

The classical and quantum domains are defined by labelling all ions as either classical or quantum, and associating spatial domains with the coordinates of each, denoted $\{\mathbf{R}_{ci\alpha}\}$ and $\{\mathbf{R}_{qi\alpha}\}$ respectively. The quantum domains are assumed to be small, to allow practical calculation of the electronic structure. In principle there could be several disconnected quantum domains, but to simplify the discussion we consider only one. It is assumed that initially the two sets are contiguous with a smooth interface and that diffusion or migration between them is not significant over the times of interest. In addition to the ions in the quantum domain, there are m electrons where m is determined by a condition on the charge of the quantum domain, here taken to be neutral. The total average electron charge density is then decomposed as

$$\bar{\rho}_e(\mathbf{r}, t) = \bar{\rho}_e(\mathbf{r}, t) (\chi_{\mathcal{Q}}(\mathbf{r}) + \chi_{\mathcal{C}}(\mathbf{r})) \equiv \bar{\rho}_{eq}(\mathbf{r}, t) + \bar{\rho}_{ec}(\mathbf{r}, t), \quad (19)$$

where $\chi_{\mathcal{Q}}(\mathbf{r})$ and $\chi_{\mathcal{C}}(\mathbf{r})$ are characteristic functions for \mathcal{Q} and \mathcal{C} . The boundaries of the quantum spatial domain \mathcal{Q} are constrained by the choice of ions and total electron charge

$$me = \int_{\mathcal{Q}} d\mathbf{r} \bar{\rho}_{eq}(\mathbf{r}, t), \quad (20)$$

where \mathcal{Q} encloses all $\{\mathbf{R}_{qi\alpha}\}$ (this leaves some flexibility to define smooth interfaces). The complement of this is the classical domain \mathcal{C} . This gives a corresponding decomposition of the total ion potential energy function for the ions V_i (ion - ion Coulomb interactions plus U_i of (14)) so that (13) becomes

$$\partial_t D_i + \{(K_i + V_{ic} + V_{iq}), D_i\} = 0, \quad (21)$$

where K_i is the ion kinetic energy and

$$V_{ic} = \frac{1}{2} \int_{\mathcal{C}} d\mathbf{r} \rho_i(\mathbf{r}) \left(\int_{\mathcal{C}} d\mathbf{r}' \frac{1}{|\mathbf{r} - \mathbf{r}'|} (\rho_i(\mathbf{r}') - \delta(\mathbf{r} - \mathbf{r}') + \bar{\rho}_{ec}(\mathbf{r}', t)) + \int_{\mathcal{Q}} d\mathbf{r}' \frac{1}{|\mathbf{r} - \mathbf{r}'|} (\rho_i(\mathbf{r}') + \bar{\rho}_{eq}(\mathbf{r}', t)) \right), \quad (22)$$

and

$$V_{iq} = \frac{1}{2} \int_{\mathcal{Q}} d\mathbf{r} \rho_i(\mathbf{r}) \left(\int_{\mathcal{Q}} d\mathbf{r}' \frac{1}{|\mathbf{r} - \mathbf{r}'|} (\rho_i(\mathbf{r}') - \delta(\mathbf{r} - \mathbf{r}') + \bar{\rho}_{eq}(\mathbf{r}, t)) + \int_{\mathcal{C}} d\mathbf{r}' \frac{1}{|\mathbf{r} - \mathbf{r}'|} (\rho_i(\mathbf{r}') + \bar{\rho}_{ec}(\mathbf{r}', t)) \right). \quad (23)$$

The first terms of the integrands on the right sides of (22) and (23) represent the interactions of the ions with a given subsystem in the presence of the average electronic charge density of that subsystem. The second terms represent the interactions of those ions with their complementary subsystem. Half of the ion - ion potential energy between the two subsystems has been associated with each potential in this decomposition so that the total force acting on the quantum domain by the classical domain is equal and opposite to that on the classical domain due to the quantum domain.

The potential V_{ic} is due to ions. By definition these ions are in near equilibrium states and therefore this part of the potential should be represented well by classical pair potentials of the form (18), with appropriately chosen parameters as discussed below. The potential V_{iq} is due to ions in the quantum domain. As this is the domain that can be far from equilibrium the average electronic charge densities must be calculated in detail from the quantum description (15). There are two parts to this charge density affecting the ions in the quantum domain, that due to the m electrons of the quantum domain $\bar{\rho}_{eq}(\mathbf{r}, t)$, and that due to the surrounding classical domain $\rho_i(\mathbf{r}) + \bar{\rho}_{ec}(\mathbf{r}, t)$. The equation governing the m electrons of the quantum domain is coupled to this same classical domain average charge density. The scheme proposed here consists of modeling this charge density $\bar{\rho}_{ec}(\mathbf{r}, t)$ as an accurate and practical representation for the environment of the quantum domain, allowing calculation of $\bar{\rho}_{eq}(\mathbf{r}, t)$ and therefore determining both V_{iq} and V_{ic} .

In summary, the multiscale model is obtained by replacing the ion - ion contribution in the classical domain (the first term on the right side of (22)) by suitably parameterized pair potentials, and constructing an accurate approximate calculation of the electron density in the quantum domain. The latter entails a representation of the effects of the electron density in the classical domain on charges in the quantum domain. In this way the potentials of (22) and (23) are entirely determined. The details of this construction are addressed in the following sections.

IV. DESCRIPTION OF THE CLASSICAL SUBSYSTEM

A. Construction of the pair potentials

The proposed method for constructing a classical pair potential for use in multiscale modeling has several components: 1) it should be constructed for accuracy of the specific properties to be studied, 2) it should be "trained" on quantum data generated in the same way as for the quantum domain at its interface, 3) it should predict accurate equilibrium structure, but include training on appropriate near equilibrium states as well, and 4) simplicity of form for parameterization and implementation in MD codes should be maintained.

The steps in constructing a potential are the following. First the specific quantum method to be used in the multiscale modeling is identified (below, transfer Hamiltonian or density functional) and applied to a large cluster or representative sample of the solid to be modeled. The forces on atoms for both equilibrium and near equilibrium states are then calculated quantum mechanically. Next, a simple functional form for the pair potentials with the correct physical shape (e.g., one of the existing phenomenological forms) is chosen and the parameters controlling that shape selected for optimization. The forces on the ions are calculated for these chosen potentials at the configurations used in the quantum force calculations, and compared with those quantum forces. The parameters are adjusted for a best fit to the quantum force data. When a good fit has been obtained, the potential energy at equilibrium is tested for stability using a gradient algorithm to establish that a local minimum of the potential has been obtained. Finally, the property of interest (e.g., some linear response) is tested by comparing its calculation using MD simulation with the fitted potentials and that with the quantum forces. If necessary, the fitting procedure can be repeated with differing weights for the quantum force data in equilibrium and near equilibrium states, or other additional input from the quantum calculations.

A more detailed discussion of the flexibility in this procedure is described for the example of the next section. It entails some art as well as science in choosing the optimization methods and applying them. In that example, it was found that some repeated combination of genetic algorithms and scaling provided the accuracy required. The primary result of this approach is a classical pair potential which gives the properties of interest by design, that match those being calculated quantum mechanically across the interface - for near equilibrium states.

B. Effects of the environment

The above construction describes the modeling of the first term on the right side of (22) where both the ions and the average electron charge density refer to the classical domain, assumed in a near equilibrium state. The second term involves a coupling to ions and average charge density (now the ground state charge density) in the quantum domain $\bar{\rho}_{eq}(\mathbf{r}, t)$. This charge density is computed for the forces in the quantum domain (next section) and hence the second term of (22) is known as well. Thus, the potential energy for the ions of the classical domain is determined from synthesized pair potentials among the ions and electrons of the classical domain, plus an interaction with the electrostatic potential of the ions and average electron charge density of the quantum domain. However, in the examples discussed below the coupling of the classical domain ions to the quantum domain is simplified by using the same pair potentials as for ions within the classical domain. This is expected to be quite accurate if the quantum domain charge density is not distorted very much from the near equilibrium states, since the potentials are trained to be equivalent to the charge density in the near equilibrium domain.

V. DESCRIPTION OF THE QUANTUM SUBSYSTEM

The quantum domain is a subsystem of m electrons localized about the designated ions defining that domain. Consider the reduced density operator for m electrons defined by

$$D_e^{(m)} = Tr_e^{N_e-m} D_e \quad (24)$$

More specifically, this partial trace is defined in coordinate representation by

$$\langle \mathbf{r}_1, \dots, \mathbf{r}_m | D_e^{(m)} | \mathbf{r}'_1, \dots, \mathbf{r}'_m \rangle = \int d\mathbf{r}_{m+1} \dots d\mathbf{r}_{N_e} \langle \mathbf{r}_1, \dots, \mathbf{r}_m, \mathbf{r}_{m+1}, \dots, \mathbf{r}_{N_e} | D_e | \mathbf{r}'_1, \dots, \mathbf{r}'_m, \mathbf{r}_{m+1}, \dots, \mathbf{r}_{N_e} \rangle \quad (25)$$

Clearly the full exchange symmetry among all N_e electrons is preserved. However, this reduced density operator is not specific to the quantum domain defined above only. For example, the diagonal elements $\langle \mathbf{r}_1, \dots, \mathbf{r}_m | D_q | \mathbf{r}_1, \dots, \mathbf{r}_m \rangle$ give the probability density to find m electrons at the specified positions, and the latter can be chosen anywhere inside the system. Thus, only when the positions are restricted to the quantum domain \mathcal{Q} does this reduced density operator represent the electrons of that domain. Similarly, if $\rho_e^{(m)}(\mathbf{r})$ is the

charge density operator for m electrons its average is

$$\bar{\rho}_e^{(m)}(\mathbf{r}) = \text{Tr}_e \rho_e^{(m)}(\mathbf{r}) D_e = \text{Tr}_e^m \rho_e^{(m)}(\mathbf{r}) D_e^{(m)} \quad (26)$$

where the trace in the second equality is over m degrees of freedom. This average charge density represents the average contribution of m electrons at any point \mathbf{r} . Both $\langle \mathbf{r}_1, \dots, \mathbf{r}_m | D_q | \mathbf{r}_1, \dots, \mathbf{r}_m \rangle$ and $\bar{\rho}_e^{(m)}(\mathbf{r})$ change with \mathbf{r} since there is an absolute reference background set by the functional dependence on the ion charge density. Consequently, in all of the following discussion of this section $\langle \mathbf{r}_1, \dots, \mathbf{r}_m | D_q | \mathbf{r}_1, \dots, \mathbf{r}_m \rangle$ and $\bar{\rho}_e^{(m)}(\mathbf{r})$ are considered only for positions within the chosen quantum domain. Accordingly, this coordinate representation $\{|\mathbf{r}_1, \dots, \mathbf{r}_m\rangle\}$ defines an m electron Hilbert space of functions defined over the quantum domain \mathcal{Q} . In this context $D_e^{(m)}$ becomes the reduced density operator for the quantum domain and $\rho_e^{(m)}(\mathbf{r})$ its charge density operator

$$D_e^{(m)} \rightarrow D_q, \quad \rho_e^{(m)}(\mathbf{r}) \rightarrow \rho_{eq}(\mathbf{r}). \quad (27)$$

The equation determining the reduced density operator for the quantum subsystem follows directly from this definition and Eq. (15) for D_e

$$\frac{i}{\hbar} [(K_e + V_{eq}), D_q] = 0. \quad (28)$$

where K_e is the kinetic energy for the m electrons and

$$V_{eq} = \frac{1}{2} \int_{\mathcal{Q}} d\mathbf{r} \rho_{eq}(\mathbf{r}) \left(\int_{\mathcal{Q}} d\mathbf{r}' \frac{1}{|\mathbf{r} - \mathbf{r}'|} (\rho_{eq}(\mathbf{r}') - \delta(\mathbf{r} - \mathbf{r}') + \bar{\rho}_i(\mathbf{r}')) + \int_{\mathcal{C}} d\mathbf{r}' \frac{1}{|\mathbf{r} - \mathbf{r}'|} (\bar{\rho}_{ec}(\mathbf{r}') + \bar{\rho}_i(\mathbf{r}')) \right). \quad (29)$$

(The contribution from $\bar{\rho}_{ec}(\mathbf{r}')$ in the second term actually should be a conditional average; the same mean field approximation as in (11) has been introduced here for consistency). The first term on the left side of (29) describes the isolated quantum subsystem, composed of the Coulomb interactions among the m electrons and their coupling to the average charge density of the ions in the quantum domain. The second term is the interaction of these electrons with their environment, the total average charge density of the classical domain.

There are two distinct types of contributions from this charge density of the classical domain. The first is associated with a subset of ions at the border of the QM/CM domains which describe chemical bonds in the full quantum solid. These ions locate regions where there is a highly localized electron charge density shared with the quantum domain, including

both strong correlation and exchange effects, localized and non-uniform. The second type of contribution is associated with the remaining border ions and those charges more distant. In this second case the quantum correlation and exchange effects of the first type are much weaker, and the dominant effect is that of a polarized charge density due to the ions and electrons.

These two types of effects of the environment can be identified by separating the total charge density for the classical domain in (29) into domains centered on the border ions responsible for bonding, and their complement

$$\bar{\rho}_c(\mathbf{r}) \equiv \bar{\rho}_{ec}(\mathbf{r}) + \bar{\rho}_i(\mathbf{r}) = \sum_{\alpha \in \mathcal{V}} \chi(|\mathbf{r} - \mathbf{R}_\alpha|) \bar{\rho}_c(\mathbf{r}) + \Delta\bar{\rho}_c(\mathbf{r}) \quad (30)$$

where it is understood that \mathbf{r} is in the classical domain. The set of border ions for which a bond has been broken in identifying the quantum domain is denoted by \mathcal{V} . Also, $\chi(|\mathbf{r} - \mathbf{R}_\alpha|)$ is a characteristic function specifying a domain centered on \mathbf{R}_α such that it does not overlap neighboring ions. Its size is taken large enough to incorporate the bound electrons forming the "atom" for this ion in the quantum solid. The second term $\Delta\bar{\rho}_c(\mathbf{r})$ is the charge density for all remaining ions and electrons of the classical environment.

A. Coulomb effects of environment

By its definition, the averaged charge density $\Delta\bar{\rho}_c(\mathbf{r})$ does not include the contributions to chemical bonding with the quantum domain required for its valency. Hence the electrostatic potential associated with it can be expected to have a regular multipole expansion

$$\int_{\mathcal{Q}} d\mathbf{r}' \frac{1}{|\mathbf{r} - \mathbf{r}'|} \Delta\bar{\rho}_c(\mathbf{r}) \rightarrow \frac{\hat{\mathbf{r}} \cdot \mathbf{d}}{r^2} + .. \quad (31)$$

The leading monopole term is zero due to charge neutrality of the classical subsystem, and the dipole moment \mathbf{d} for the entire environment is

$$\mathbf{d} = \int d\mathbf{r}' \mathbf{r}' \Delta\bar{\rho}_c(\mathbf{r}). \quad (32)$$

These results are still quite formal but they provide the basis for the phenomenology proposed for this part of the modeling: Replace all effects of the classical environment on the quantum system, exclusive of bonding, by an effective dipole representing the polarization of the medium by the quantum domain. The origin of this dipole in the above analysis

shows that in general it will depend on the geometry and the state of both the classical and quantum domain (e.g., it will change under conditions of strain). In the phenomenological application of this prescription the dipole must be supplied by some simpler means since the electronic contribution to $\Delta\bar{\rho}_c(\mathbf{r})$ is not known (for example, see reference²⁴).

B. Electron exchange with environment

The contributions from $\bar{\rho}_c(\mathbf{r})$ in the regions where bonds have been cut require a more detailed treatment. Clearly, a necessary condition is that valence saturation should be restored in the quantum domain. However, that is not sufficient to assure the correct charge density there nor the correct forces within that domain. Instead, the charge density near the border ions responsible for bonding should induce a realistic charge density within the quantum domain. To see how this can be done first write the contribution from one such border ion to (30) as

$$\int d\mathbf{r}' \frac{1}{|\mathbf{r} - \mathbf{r}'|} \chi(|\mathbf{r}' - \mathbf{R}_\alpha|) \bar{\rho}_c(\mathbf{r}) \equiv \phi_{p\alpha}(\mathbf{r}) \quad (33)$$

The potential $\phi_{p\alpha}(\mathbf{r})$ represents the actual electrostatic and exchange effects of the nucleus of the border of the quantum domain. This is comprised largely of the ion at the site plus its closed shell electrons distorted by exchange and correlation effects of the site in the quantum domain with which it is bonding. Consequently, an appropriate pseudo-potential is introduced at each such border ion whose behavior in the direction of the quantum system is the same as that of the actual ion. These ions plus their pseudo-potentials will be called "pseudo atoms".

To accomplish this, an appropriate candidate for the pseudo atom is chosen based on valency of the particular pair of border ion and its neighbor in the quantum domain. Next, a large molecule or small cluster containing that bonding pair is chosen for training the pseudo atom. The bond is then broken and the relevant member of the pair replaced by the pseudo atom. The training consists of parameterizing the pseudo atoms' effective potential to give the same forces as in the original cluster. For example, the pseudo atom might consist of an ion plus its closed shell electrons chosen to satisfy the valency for the bond broken. The adjustable parameters could refer to a characterization of the closed shell electron distribution. In this way, it is assured that the pseudo atom not only gives the

correct saturation of the dangling bond but also reproduces the forces within the cluster and hence gives a realistic representation of the charge distribution between the chosen pair. For the small training cluster (e.g., Figure 6), forces are determined both at equilibrium and under strain to within about one tenth percent. The primary assumption is that the bonding of interest is a local effect, so that the pseudo atom trained in the cluster will have a similar accuracy when used in the bulk solid. The training depends on the particular quantum method used to describe the solid, and is illustrated in more detail for the specific example considered in the later sections.

In summary, the environmental effects on the quantum system are accounted for approximately by a dipole representing its polarization and a collection of pseudo atoms located at the sites of ions where bonds have been cut

$$V_{eq} \rightarrow \frac{1}{2} \int_{\mathcal{Q}} d\mathbf{r} \rho_{eq}(\mathbf{r}) \left(\int_{\mathcal{Q}} d\mathbf{r}' \frac{1}{|\mathbf{r} - \mathbf{r}'|} (\rho_{eq}(\mathbf{r}') - \delta(\mathbf{r} - \mathbf{r}') + \bar{\rho}_i(\mathbf{r}')) + \frac{\hat{\mathbf{r}} \cdot \mathbf{d}}{r^2} + \sum_{\alpha \in \mathcal{V}} \phi_{p\alpha}(\mathbf{r}) \right). \quad (34)$$

This model now allows solution to (28) for the electron distribution the quantum domain, including its coupling to the classical environment. Then $\bar{\rho}_{eq}(\mathbf{r})$ is calculated from (26) and (27). Finally, the desired potentials V_{ic} and V_{iq} of (22) and (23) are fully determined

$$V_{ic} = \frac{1}{2} \sum_{i,j} \sum_{\alpha}^{N_i} \sum_{\beta}^{N_j} V_{ij} (|\mathbf{R}_{i\alpha} - \mathbf{R}_{j\beta}|) + \frac{1}{2} \int_{\mathcal{C}} d\mathbf{r} \rho_i(\mathbf{r}) \int_{\mathcal{Q}} d\mathbf{r}' \frac{1}{|\mathbf{r} - \mathbf{r}'|} (\rho_i(\mathbf{r}') + \bar{\rho}_{eq}(\mathbf{r}', t)), \quad (35)$$

and

$$V_{iq} = \frac{1}{2} \int_{\mathcal{Q}} d\mathbf{r} \rho_i(\mathbf{r}) \left(\int_{\mathcal{Q}} d\mathbf{r}' \frac{1}{|\mathbf{r} - \mathbf{r}'|} (\rho_i(\mathbf{r}') - \delta(\mathbf{r} - \mathbf{r}') + \bar{\rho}_{eq}(\mathbf{r}, t)) + \frac{\hat{\mathbf{r}} \cdot \mathbf{d}}{r^2} + \sum_{\alpha \in \mathcal{V}} \phi_{p\alpha}(\mathbf{r}) \right). \quad (36)$$

The solution to the classical ion motion (21) can then proceed via MD simulation. This completes the proposed scheme for multiscale modeling of the idealized quantum solid. Rather than critique further the assumptions made in this abstract context, the scheme is discussed in more detail for a specific application to an SiO_2 nanorod.

VI. SiO_2 NANOROD - A CRITICAL TEST

The modeling scheme of the previous sections is now illustrated in detail and tested critically for a model solid consisting of a silica nanorod²⁶, shown in Figure 1. It consists of 108 Si and O ions with the stoichiometric ratio of one silicon to two oxygens, a stack

of six Si_6O_6 rings sharing both above and below a ring of oxygen atoms. To saturate overall valency the nanorod is terminated with end cap rings whereby each silicon atom of the terminating ring is connected by bridging oxygen or two interstitial oxygens. The size of this nanorod can be readily adjusted by adding or removing Si_6O_6 planar rings with corresponding O atoms. Many of the results reported here have been studied for larger rods as well²⁶. As noted in the Introduction, this system exhibits strain to fracture (Figure 1), yet it is small enough for practical application of the chosen quantum mechanics to the whole rod. Consequently, the results of modeling it as a composite rod can be tested quantitatively against the "exact" results. That is the objective of this section.

The decomposition of the rod into classical and quantum domains is accomplished by identifying the ions of one of the rings near the center as the QM domain. The rest of the ions define the classical domain. The actual geometry of the interface is chosen by charge neutrality of the quantum domain, as given by Eq.(20).

A. Transfer Hamiltonian Quantum Mechanics

At the quantum level, each possible choice for the quantum chemical method entails different approximations used to optimize the accuracy and speed of the calculations. Each approximation has its own advantages and limitations, but a general embedding scheme should be insensitive to these. Much of the previous work on multiscale modeling is based on tight binding models^{1,6} because of their ability to treat hundreds of atoms in the QM domain. However, the Hamiltonian in these models is oversimplified and cannot account for charge transfer, which is essential to bond breaking. A more complete quantum description is considered here. It is appropriate to stress at this point that the objective of the following sections is to demonstrate and test the modeling scheme for a given quantum description. That is a separate issue from the question of how accurate that description may be. To test how robust the proposed embedding scheme is, two different methods are chosen for the underlying quantum mechanical description. The first method is the Transfer Hamiltonian (TH) - Neglect of Diatomic Differential Overlap (NDDO)²⁷. The second method is the Born-Oppenheimer local spin density²⁸ within density functional theory using a generalized gradient approximation. The results obtained from the TH are described first.

The goal of the TH strategy is to provide forces for realistic MD simulations of the quality

of the coupled cluster singles and doubles method²⁹ in computationally accessible times³⁰. The TH is a low rank, self - consistent, quantum mechanical single particle operator whose matrix elements are given in terms of parameterizable functions. The functional form of the TH can be chosen to be of any semi-empirical functional form, but here the NDDO form is chosen because of its better qualitative description over Intermediate Neglect of Differential Overlap (INDO) Hamiltonians³¹. The NDDO approximation restricts charge distribution to basis functions on the same center, so this has at most two-atom interactions. Because of its NDDO form it is anticipated that the parameters fit to coupled cluster data are saturated for small cluster size and that these parameters can then be transferred to extended systems. This transfer might be considered an example of serial multiscale-modeling.

To apply the TH to silica systems for studying complex processes such as fracture or hydrolysis where the role of electrons is important, Taylor *et al.*²⁷ parameterized the TH for the following reactions $Si_2H_6 \rightarrow 2SiH_3$, $Si_2O_7H_6 \rightarrow Si(OH)_3 + SiO(OH)_3$ (radical mode of dissociation), and $Si_2O_7H_6 \rightarrow {}^+Si(OH)_3 + {}^-OSi(OH)_3$ (ionic mode of dissociation). By describing the two different dissociation pathways for $Si_2O_7H_6$, electron state specificity is systematically introduced into the TH model. Since fracture is expected to involve a variety of dissociations this TH model is expected to be appropriate for study of strained conditions as is done here. Thus the parameterized TH model is expected to provide accurate results for such processes, while requiring only the computational intensity of semi-empirical methods which are orders of magnitude less demanding than coupled cluster calculations on the same systems. In the next few subsections, the charge densities and forces that arise from the TH are the reference data by which the proposed method for multiscale modeling is judged.

B. Pair Potentials for the Classical Domain

The method that we propose for constructing a classical pair potential has been previously presented in detail²⁵, so only a brief summary is given here. The functional form for the potential is chosen to be one that is commonly used in the literature. In the case of silica, this is the TTAM³⁴ and BKS³⁵ forms which are pair potentials comprised of a Coulombic interaction, a short-range exponential repulsion, and a van der Waals attraction (the last two terms are collectively known as the 'Buckingham' potential)

$$V_{ij}(r) = \frac{q_i q_j}{r} + a_{ij} e^{-b_{ij} r} - \frac{c_{ij}}{r^6} \quad (37)$$

There are 10 free parameters as the charge neutrality of the SiO_2 unit requires that $q_{Si} = -2q_O$, so that a_{ij} , b_{ij} , and c_{ij} for each atom pair and one charge define the potential. For the purposes here, this potential is used to generate the dynamics (MD simulations) so that forces have been used as the property "training" the potential (determining the free parameters). More specifically, force data from the silica nanorod calculated with the TH at equilibrium and a few small strain configurations have been used.

Fitting a set of ten parameters from hundreds of data points requires an optimization approach that is capable of exploring a large parameter space efficiently without being trapped in local minima. For this task, a genetic algorithm (GA) has been chosen as detailed in reference²⁵. The GA generates a number of sets of parameters of a given fitness which are then tested using a standard geometry optimization technique (BFGS³⁸) to ensure that the parameterization gives a stable equilibrium configuration. The parameter set that gives a geometry closest to the TH nanorod is then chosen and rescaled to reproduce the equilibrium structure to within a few percent. (See the appendix of reference²⁵ for details of the rescaling used.) Table I presents the final parameters obtained compared to the TTAM and BKS parameters. Table II shows that the new classical potential reproduces the nanorod structure to within a few percent compared to larger discrepancies with the two standard potentials. The shapes of these three potentials are shown in Figure 2 for the Si-O pair interaction.

Finally, the small strain elastic behavior of this new potential is studied. This is accomplished using MD simulation of uniaxial strain along the long axis (z) of the silica nanorod at a strain rate of 25 m/s. The integration is done using 2 fs time steps and a temperature of 10 K enforced by velocity rescaling. Figure 3 shows the resulting stress-strain curves for small strains up to 5%. It is noted that the new potential indeed reproduces the linear elastic response (Young's modulus) behavior of the underlying TH while the TTAM and BKS potentials are somewhat stiffer.

A key to successful multiscale modeling lies in the consistent embedding of a QM domain in its classical MD region. This requires that the CM region have the same structure and elastic properties as the QM domain. The potential obtained in this section meets these criteria for the silica nanorod. Essentially, a classical representation of the TH silica nanorod has been found for both equilibrium and near-equilibrium configurations.

TABLE I: Potential Parameters.

Parameter	TTAM	BKS	New potential
q_{si}	2.4	2.4	2.05
q_o	-1.2	-1.2	-1.025
a_{oo}	1756.98	1388.773	39439.87
b_{oo}	2.846	2.760	4.66
c_{oo}	214.75	175.00	5.85
a_{osi}	10722.23	18003.757	240101.9
b_{osi}	4.796	4.873	7.88
c_{osi}	70.739	133.538	2.06
a_{sisi}	$8.73E + 8$	0	27530.45
b_{sisi}	15.22	0	21.42
c_{sisi}	23.265	0	1.55

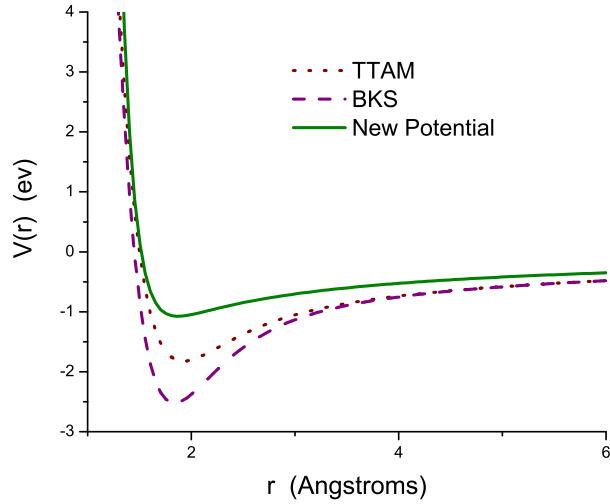


FIG. 2: (color online) Si-O pairwise interactions for the three potentials

C. The Quantum Domain

A proper description of the quantum domain requires incorporating two kinds of environmental effects: a short-range electronic exchange interaction and long-range Coulombic

TABLE II: Structure of the Nanorod from the Different Potentials.

Bond lengths and angles (\circ)	TH	New TH potential	% error	TTAM	% error	BKS	% error
<i>In Silica Plane</i>							
$Si - O$	1.641	1.642	0.04	1.65	0.76	1.611	1.5
$< Si - O - Si$	170.06	173.7	2.14	162.9	4.2	161.1	5.2
<i>Between Planes</i>							
$< Si - O - Si$	103.8	104.3	0.4	104.6	0.7	104.9	1.04
<i>End caps</i>							
$Si - O$	1.71	1.67	2.5	1.67	2.5	1.62	5.1
$< Si - O - Si$	102.03	103.2	1.14	100.6	1.45	100.8	1.23
Length	16.49	16.34	0.9	16.31	1.1	15.86	3.8
Diameter	6.55	6.54	0.15	6.57	0.35	6.41	2.0

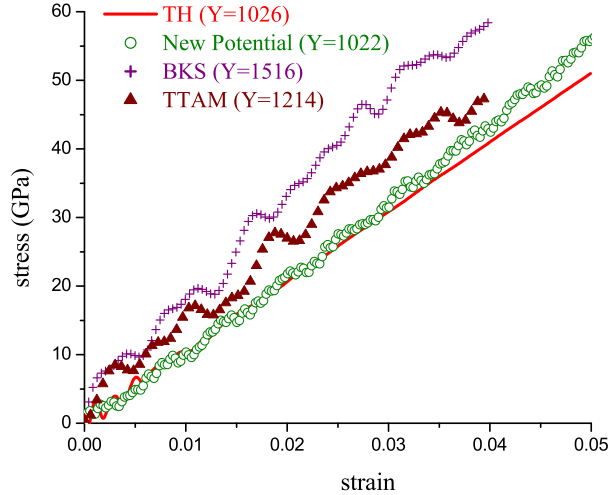


FIG. 3: (color online) Stress-strain curves for the different potentials and for TH quantum mechanics

interactions. Most previous studies of QM/CM simulations have focused on the former and have neglected the long-range interactions. It will be shown here that both kinds of interactions must be taken into account for an accurate description of forces and charge densities in the QM domain. This subsection first reviews briefly the various termination schemes used in the literature to treat the bond cutting region. Then, the method proposed here

for construction of a pseudo-atom to saturate dangling bonds is described, together with modeling the rest of the CM environment by lowest order multipoles. The charge densities and forces in the QM domain obtained from our scheme of pseudo-atoms and dipoles with those obtained from the conventionally used link atoms (bond saturation with hydrogen atoms) and dipoles are compared to the "exact" TH reference data for the entire nanorod.

Over the past decade there have been numerous proposals for different types of termination schemes to accommodate dangling bonds. Only a few of the more relevant ones are noted for context. (i) Link Atom method: This commonly used method is the Link Atom method, presented by Singh and Kollman³⁹. In this method, hydrogen atoms are added to the CM side of broken covalent bond to satisfy the valency of the QM system. There are many variations within the implementation of the LA method, for example, the double Link Atom method⁴⁰, the Add-Remove Link Atom method⁴¹ or the Scaled-Position-Link-Atom Method (SPLAM)²¹. In the present work, the hydrogen atoms are placed at a fixed distance of 0.97 Å from the cut Si bond. (ii) Connection Atom method⁴⁶: A connection atom is developed to saturate a C-C bond, such that the connection atom mimics the effect of a methyl group. This connection atom interacts with the QM atom quantum mechanically and the interactions with the CM atoms are handled classically using a carbon force field. The parameters of the connection atom are determined using semi-empirical methods⁴⁷ such as AM1, MNDO or PM3 designed to reproduce theoretical QM data for energies, geometry and net charges. About 30 different methyl hydrocarbons were used as reference molecules. The parameters adjusted are the orbital exponent, one-center one-electron energy, one center two-electron integral, resonance parameter, and repulsion term. The mathematical functional forms of these parameters can be found in any book on semi-empirical theory⁴⁷ or papers by Dewar and Theil⁴⁸.

There are numerous other termination schemes for the QM/CM boundary like the 'pseudobond' scheme⁴⁹, 'IMOMM'^{50, 51} and 'ONIOM'^{52, 50, 53} procedures, 'effective group potential (EGP)'⁵⁴. However these methods are not discussed here.

The method proposed here will be referred to as the "pseudo-atom" method. In the present case it is based on the TH approach for saturating a bond terminating in Si (in silica systems). The training cluster is a pyrosilicic acid molecule (Figure 4). The part of the molecule within the dotted lines is replaced by a fluorine (F) atom whose NDDO parameters are then adjusted to give the correct QM forces (which implies correct geometry

as well) and charge density in other parts of the molecule (outside the dotted lines). The pseudo atom is placed at the same position as the neighboring CM atom (O in this case) in the bond being cut and hence geometry optimization as in the LA method is not required. The specific NDDO parameters modified are: one-center-one-electron integrals, Coulomb integrals, exchange integral, and two-center-one-electron resonance integrals⁴⁸. This method is similar to the previously described connection atom developed in reference⁴⁶. However the advantage of using pseudo-atoms is that they are trained to give the correct QM forces and charge densities for both the equilibrium Si-O bond being cut and for small distortions (up to 3 – 4% from the equilibrium) in the Si-O bond length as well. This allows use of the pseudo-atoms even while studying dynamics in the system. To test this method, the

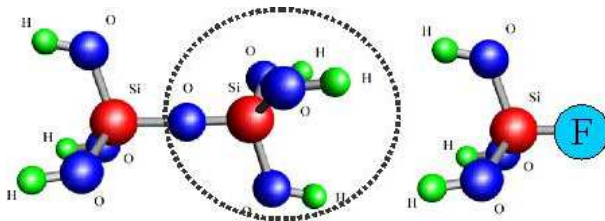


FIG. 4: (color online) Training of Pseudo-atom on Pyrosilicic acid

actual charge density from the TH method is calculated instead of the more commonly used Mulliken populations⁵⁵, which are known to have several common problems (e.g., equal apportioning of electrons between pairs of atoms, even if their electronegativities are very different).

The remainder of the environment is represented as two dipoles for the top and bottom portions of the rod (Figure 5). The values of the dipole have been calculated using the TH-NDDO charge density for these two portions of the rod. These domains are taken to be charge neutral, but are polarized by the presence of the QM domain. The validity of the approximation by dipoles has been checked by comparing the force on an Si nuclei of the ring due to all charges and that due to the dipole, with excellent agreement. Constructing the full system as a composite of a QM domain terminated by pseudo atoms and embedded in dipolar fields leads to the forces displayed in Figure 6. It is found that the normalized difference of charge density is reproduced to within 0.1% in the plane of the ring²⁴.

This scheme was found to be applicable to both equilibrium and strained configurations, as illustrated in Figure 6 for the following cases: a) equilibrium, b) the ring of the QM

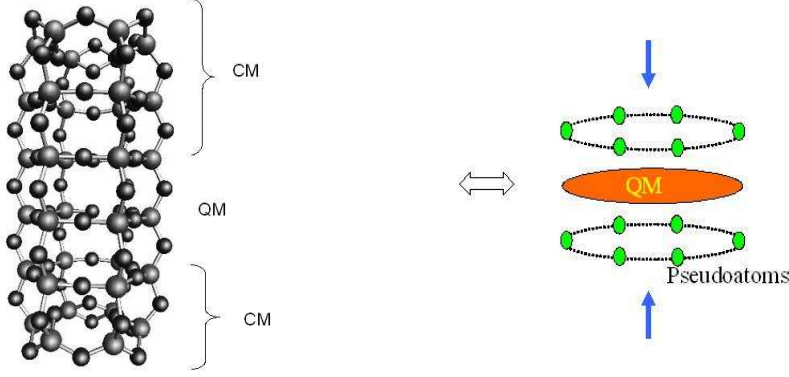


FIG. 5: (color online) Embedding Scheme: Approximating the CM region by pseudo-atoms and dipoles

domain radially expanded by 5%, and c) a distorted ring in which one Si atom is radially pushed out and one Si pushed in. Also shown are the corresponding results for a longer 10 ring rod (cases d),e), and f)).

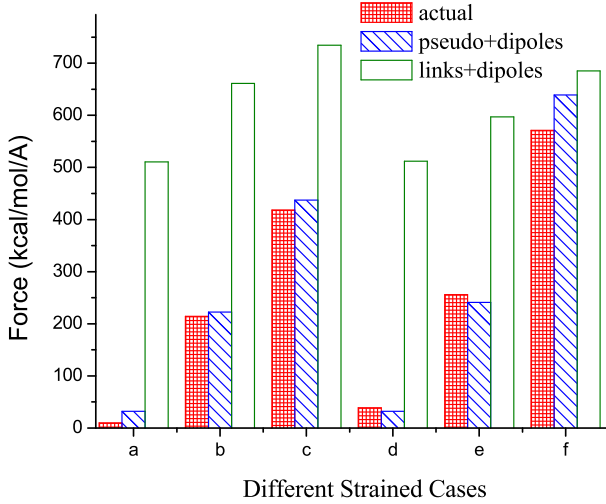


FIG. 6: Forces on Si nuclei for various cases studied

The pseudo-atoms and the dipoles reproduce the force in the QM domain within 1% error. In contrast, the LA placed at 0.97 Å from the terminating Si atom and along the Si-O bond lead to a large force on the Si atom at equilibrium, and generally poor results for the strained cases. One might argue that the LA method could be improved if placed at "optimal" positions. To test this, both the Si-H bond length as well as the alignment of the

LA was varied to give minimum force on the Si atom. This was obtained when the LA is placed at a distance of 1.45 Å from the silicon and the bond angle is decreased by about 5 degrees. Although the LA at this position gives forces comparable to those for pseudo-atoms plus the dipoles, it fails to reproduce the correct charge densities.

D. The Composite Rod

The composite rod is built by embedding the QM region in its CM environment as described in Section III. The forces on the atoms in the CM region are calculated from the pair potential developed in IV B above, while the forces on the atoms in the QM domain are obtained from the charge density calculated by the TH method as described in VI C . An important test of the composite rod is its indistinguishability from the TH rod for near equilibrium states, i.e. its structure and elastic properties.

The structural properties (bond lengths, bond angles) have an accuracy comparable to that of the purely classical rod described using this pair potential (Table II). Consequently, attention here will be focused on the elastic properties. Figure 7 shows the stress-strain behavior of the nanorod obtained from three different methods: (i) quantum mechanics TH method for the entire rod, (ii) pair potentials for the entire rod, and (iii) the composite rod constructed as described above. The three overlaying curves (measured at 0.01K) indicate that the composite rod is identical to the rod obtained from TH and the pair potential nanorod in terms of small strain elastic properties and structure. The stress-strain results shows the success of our multiscale method indicating that the composite rod is indistinguishable from the underlying quantum mechanics for states near equilibrium.

E. Notched Nanorod

The elastic properties of the composite rod obtained from both of these potentials do not agree beyond 10% strain. This is because the pseudo-atoms, trained at regions only close to the equilibrium configuration, fail to give the correct charge densities at such high strains. This diagnosis was checked by comparing the charge density in the QM domain of the 12% strained rod with that of equilibrium configuration and a difference of 6% was found. Retraining of the pseudo-atoms improve the stress-strain performance of the composite rod

beyond a strain of 10% is possible, but this was not done because of the large strains involved. Real systems like glasses have many inherent defects which act as stress concentrators that cause the material to break at much lower strains than observed for the nanorod (with a yield stress of about 190 GPa).

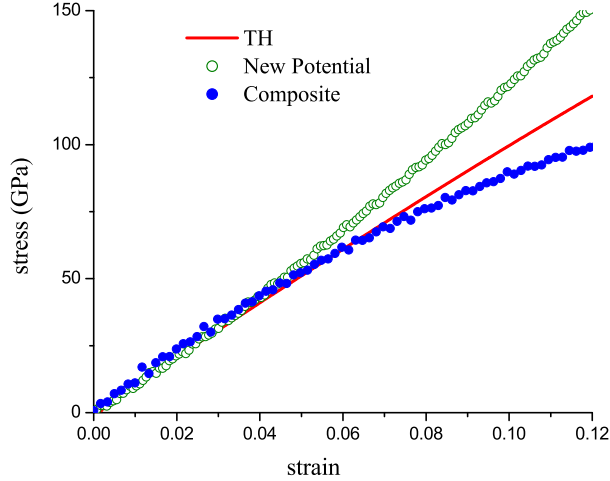


FIG. 7: (color online) Stress-strain curve for the TH (quantum), new potential (classical), and composite rods

To illustrate this, a defect notch was placed in the 108 atom nanorod by removal of an oxygen atom as shown in Figure 8. The MD stress-strain curves for this notched rod were found using TH quantum mechanics, the trained classical potential, and the composite. We note that the presence of only a small defect can significantly reduce the yield stress of the material and make it more prone to fracture. The TH curve for the defect-free rod is plotted in the same figure to contrast the value of the yield stress. As can be seen there is a reduction of ~ 60 GPa in the yield stress. For the composite rod in this case, the QM domain was chosen to consist of 2 silica planes and the intermediate 5 oxygen atoms (see Figure 8), so that the defect could be located in the QM region. The stress - strain curve for this composite notched rod agrees well with that for the TH quantum calculation up to 10% strain. Above 4% strain the curve for the composite notched nanorod follows that of the TH instead that of the trained classical potential nanorod, showing that the composite rod is representing the "real" material. This is exactly what is required of multiscale modeling.

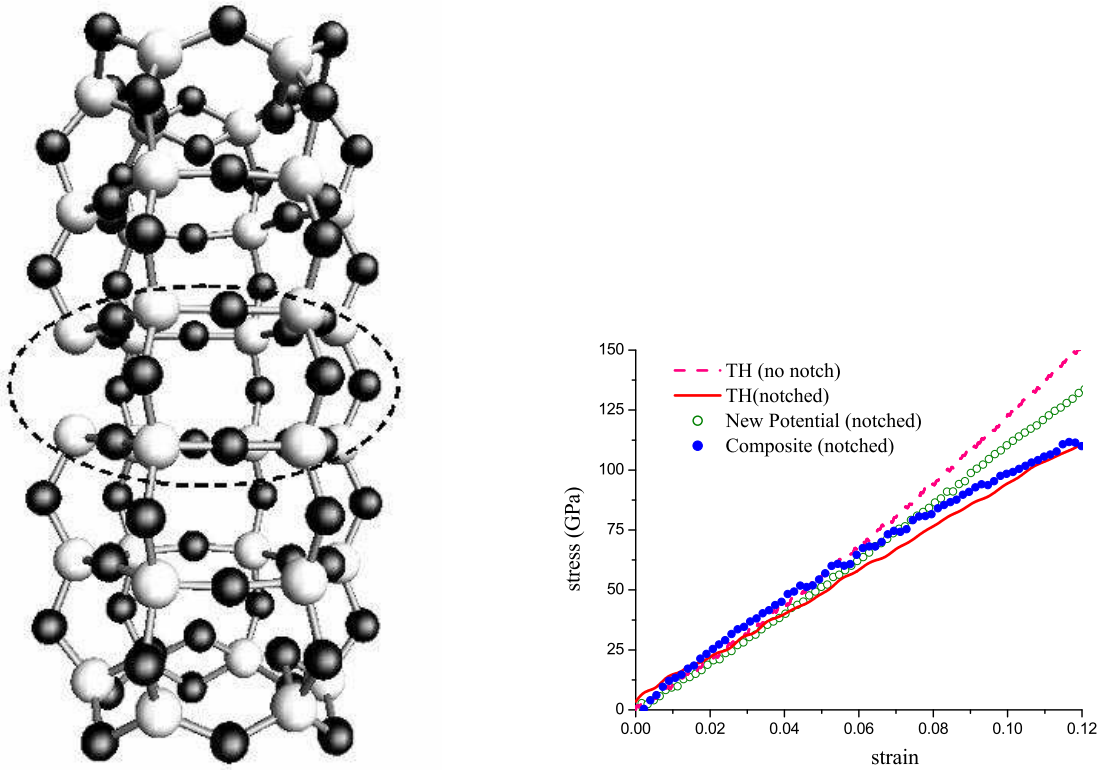


FIG. 8: (color online) The notched nanorod and corresponding stress-strain curve

F. DFT Quantum Mechanics

A proper multiscale modeling procedure should be independent of the choice of underlying quantum mechanical method. To test the method proposed here, the analysis of subsections (B)-(D) is repeated using a density functional theory (DFT) instead of the Transfer Hamiltonian as the quantum mechanical approximation. The primary results of this section are a confirmation that the isolation of the QM domain with pseudo-atoms and dipoles, plus the construction of a classical potential based on the DFT forces leads to accuracies of the same quality as those described already using the TH quantum mechanics. Hence, the multiscale modeling scheme is faithful to the chosen form for the underlying quantum mechanics in both cases. The DFT code used is a parallel multiscale program package, known as Born-Oppenheimer molecular dynamics “BOMD”²⁸. It is a generalized gradient approximation (GGA) within local spin DFT (LSDFT). A Troullier-Martin Pseudo-Potential^{56,57} is used for the effect of the chemically inert core states on the valence states. The code employs the

dual space formalism for calculation of the DFT energy. A plane wave basis set and cut-off energy of 30.84 Rydbergs is chosen.

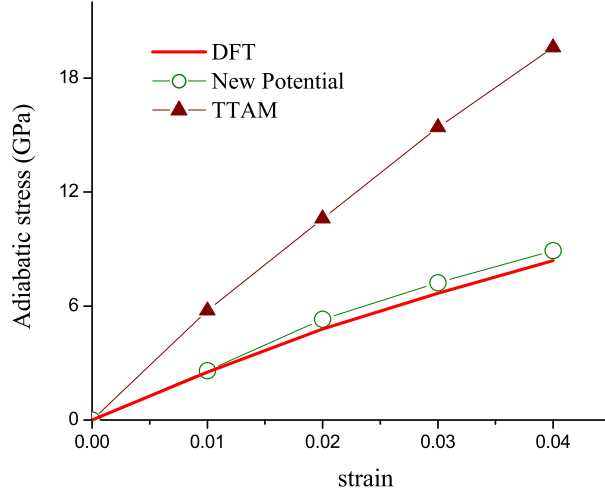


FIG. 9: (color online) Adiabatic stress curves for DFT, DFT-potential, and TTAM potential

A pseudo-atom for the quantum domain is constructed based on parameterization of the Troullier-Martin (TM) pseudopotential, using a cut-off radius of 1.5\AA . Once again the pyrosilicic acid molecule is chosen for parameterization of the fluorine-like pseudo atom and its position is constrained to be at the same place as the O atom (Figure 4). Unlike the TH-NDDO method in which both the electron-ion and electron-electron interaction parameters could be changed, in DFT only the electron-ion interactions can be modified. The three options to alter these interactions for the F atom using the TM pseudopotential are: (i) the core charge on F, (ii) omission of the non-local part in the potential, and (iii) switching the local and non-local part between s and p orbitals. All three possible choices and their combinations were explored to find the optimal reproduction of forces on the terminated Si atom in the pyrosilicic acid. The best results were obtained when the core charge is 7.0 and the non-local part is omitted. This pseudo-atom was then applied to the composite nanorod constructed as above (Figure 5). The values of the dipoles were recalculated from the charge density obtained using the DFT results for the CM portions of the rod. The force on a Si atom in the QM domain was calculated for the rod in equilibrium and all the strained cases considered in subsection C. The results obtained from a DFT calculation on the whole rod are now taken to be the "exact" reference forces. It is found that the forces and the charge

densities in the QM domain can be generated using DFT pseudo-atoms and dipoles to 1% accuracy.

Next, a new potential having the same form as TTAM is constructed to predict the same structure and elastic properties as for the QM rod. A GA with DFT force data up to 4% expansion followed by the scaling procedure is used as described in section VI B above to find the parameters for the potential. The charge on the ions is lower (as was found for TH quantum mechanics) than that given in the TTAM and BKS potentials. Also, the van der Waals interaction is much weaker than in those potentials. This is expected since the DFT forces fail to represent this effect, falling exponentially rather than algebraically with separation. The parameters for the DFT potential and a comparison of the resulting nanorod structure with that for the BKS and TTAM nanorods are given in reference²⁵. The agreement between the results from the DFT potential and DFT quantum mechanics is similar to that found in Table II for the TH quantum mechanics.

A stress strain curve for the entire rod using MD with DFT quantum mechanics is computationally too intensive. Instead, only selected equilibrium and adiabatic strain configurations were calculated with DFT. The equilibrium structure was determined by sequential DFT calculations and nuclear relaxation to find the minimum energy configuration. The strained configurations were obtained from an affine transformation of the minimum energy configuration by 1, 2, 3, and 4 %, with a single DFT calculation of forces at each of the expanded configurations. Then the average force on the Si atom in each ring of the DFT nanorod was computed for these four cases. The stresses for adiabatic configurations using DFT for the entire rod, the constructed DFT potential, and the TTAM potential were then compared (the values of stress obtained using BKS potential are similar to those of TTAM potential). The results are shown in Figure 9.

These results suggest that the multiscale modeling method proposed here is accurate for a wide range of possible choices for the underlying quantum mechanical method employed.

VII. SUMMARY AND DISCUSSION

The objectives here have been three-fold. The first was to describe the formal quantum structure for a real solid from which a practical model should be obtained through a sequence of well-identified (if not fully controlled) approximations. The second was to propose a

method for partitioning this structure into classical and quantum domains while preserving the properties of interest for the quantum structure in the replica composite solid. The final objective was a quantitative test of the proposed method by its application to a non trivial mesoscopic "solid", the SiO_2 nanorod.

For the first objective, coupled Liouville - von Neumann equations for the reduced density operators for the ions and electrons of the system were considered. Each is coupled to the other through the mean charge density of the complementary subsystem. Determination of these charge densities then becomes the central problem for further analysis. For the heavy ion component analysis by classical MD simulation provides a practical and accurate approach. The necessity for a detailed quantum treatment of the electronic charge density is the primary bottleneck for progress. For bulk samples of interest, direct application accurate quantum chemical methods are precluded, so composite constructs with smaller quantum subdomains are a potentially fruitful compromise. Here, the isolation of a quantum subdomain was accomplished by defining the reduced density matrix for electrons in the vicinity of a selected small set of ions. The corresponding Liouville - von Neumann equation describes the dynamics of those electrons and ions coupled to the remainder of the solid (the classical domain). Its environment is entirely characterized by its mean charge density. This formulation and emphasis on the charge density is a guiding feature of the subsequent approximations and modeling.

The specific method for constructing the composite solid consists of modeling the charge densities of the environment for the two subsystems. For the environment of the quantum domain the charge density is separated into that border component responsible for electronic bonding across the border, and a longer range Coulomb interaction. The former is treated in detail by pseudo atoms trained on smaller clusters to provide highly accurate local forces and charge densities. The latter is represented by leading order terms in a multi-pole expansion. The interactions within the classical domain are described phenomenologically by pair potentials. These pair potentials are designed specifically to represent selected properties determined by the quantum chemical method assumed to represent the solid. This presumes conditions such that the chosen properties have such a classical representation (e.g., near equilibrium states), and the method constitutes a "tuning" of the potential to match the quantum description on the other side of the border.

There are several critical tests of this approach, all requiring a benchmark system for

which the "exact" quantum data for the entire solid is required. This system is provided here by the nanorod for which the global quantum calculations are possible. Then, choosing a central ring as the quantum subdomain and the remainder as the classical domain many quantitative tests are possible. Some of these provided here are:

1. The charge density and forces in the central ring computed from the model are accurate to within one percent, both at equilibrium and strains up to 5%.
2. The pair potential fit to quantum data was used to construct the entire nanorod. The resulting structure and elastic properties up to 5% strain were indistinguishable from those of the quantum nanorod.
3. The proposed method was used to construct a composite classical / quantum nanorod. Again the structure and elastic properties were indistinguishable from those of the quantum nanorod.

These and other results presented above constitute a demonstration that the multiscale modeling is not creating a new solid, but rather is faithful to the real system of interest. Similar (and perhaps more physical) results were obtained for the nanorod with a defect (missing Oxygen). Finally, the entire multiscale analysis was repeated using a quite different choice for the underlying quantum mechanics with the same degree of accuracy.

The predictions of multiscale modeling for conditions of interest, states far from equilibrium, rely on the assumption that the properties calculated in the quantum subdomain are indeed those of the given quantum structure. This means that the quantum imbedding and representation of the classical domain are "passive", i.e. no new physical effects have been introduced. The method described here manifestly satisfies this constraint for the benchmark nanorod, and provides some concrete support for its use in realistic applications.

VIII. ACKNOWLEDGEMENTS

This research was supported by NSF-ITR under Grant No. DMR-0325553. The authors are indebted to S. B. Trickey, K. Muralidharan, and D. E. Taylor for helpful discussions and assistance.

-
- ¹ J. Q. Broughton, F. F. Abraham, N. Bernstein, and E. Kaxiras, Phys. Rev. B **60**, 2391 (1999).
- ² R. K. Singh and R. Bajaj, MRS Bulletin, Oct, 743 (2000).
- ³ E. Clementi, Philos. Trans. R. Soc. London, A **326**, 445 (1988).
- ⁴ G. R. Odette, B. D. Wirth, D. J. Bacon, and N. M. Ghoniem, MRS Bulletin, March, 176 (2001).
- ⁵ V. Gogonea, Internal Electronic Journal of Molecular Design, **1**, 173 (2002).
- ⁶ R. E. Rudd and J.Q. Broughton, Phys. Stat. Sol. **217**, 251 (2000).
- ⁷ A. Warshel and M. Levitt, J. Mol. Biol. **103**, 227 (1976).
- ⁸ J. Gao, Acc. Chem. Res. **29**, 298 (1996).
- ⁹ P. Amara, A. Volbeda, J. C. Fontecilla-Camps, and M. J. Field, J. Am. Chem. Soc. **121**, 4468 (1999).
- ¹⁰ G. Monard and K. M. Merz, Jr., Acc. Chem. Res. **32**, 904 (1999).
- ¹¹ S. J. Titmuss, P. L. Cummins, A. A. Bliznyuk, A. P. Rendell, and J. E. Gready, Chem. Phys. Lett. **300**, 169 (2000).
- ¹² R. B. Murphy, D. M. Philipp, and R. A. Friesner, J. Comp. Chem. **21**(16), 1442 (2002).
- ¹³ Q. Cui and M. Karplus, J. Phys. Chem. B. **106**, 1768 (2002).
- ¹⁴ G. M. Chabana and R. B. Gerber, J. Chem. Phys., **115**(3), 1340 (2001).
- ¹⁵ A. H. de Vries and P. Th. van Duijnen, Int. J. Quant. Chem. **57**, 1067 (1996).
- ¹⁶ M. A. Thompson, J. Phys. Chem. **100**, 14492 (1996).
- ¹⁷ Y. Jung, C. H. Choi, and M. S. Gordon, J. Phys. Chem. B. **105**, 4039 (2001).
- ¹⁸ M. H. Du, and H-P Cheng, J. Chem. Phys. **119**, 6418 (2003).
- ¹⁹ J. Guo and X. Xia, Science **258**, 613 (1992).
- ²⁰ J. Gao and M. Freindorf, J. Phys. Chem. A **101**, 3182 (1997).
- ²¹ M. Eichinger, P. Tavan, J. Hutter and M. Parrinello, J. Chem. Phys. **110**, 10452 (1999).
- ²² J. Sauer and M. Sierka, J. Comp. Chem., **21**, 1470 (2000)
- ²³ S. Ogata and R. Belkada, Comp. Mat. Sc. **30**, 189 (2004).
- ²⁴ A. Mallik, D. E. Taylor, K. Runge, and J. Dufty, Intl. J. Quan. Chem. **100**, 1019 (2004).
- ²⁵ A. Mallik, K. Runge, H-P Cheng, and J. Dufty, Molecular Simulations, in press.
- ²⁶ T. Zhu, J. Li, S. Yip, R. J. Bartlett, S. B. Trickey, and N. Leeuw, Molecular Simulations **29**, 671 (2003).

- ²⁷ D. E. Taylor, M. Cory, R. J. Bartlett, *Comp. Mat, Sci.*, **27**, 204 (2003).
- ²⁸ R. N. Barnett and U. Landman, *Phys. Rev. B* **48**, 2081 (1993).
- ²⁹ R. J. Bartlett in *Modern Electronic Structure Theory - Part II*, D.R Yarkony, editor (World Scientific, Singapore, 1995), p. 1047.
- ³⁰ D. E. Taylor, *The Transfer Hamiltonian: A Tool for Large Scale, Accurate, Molecular Dynamics Simulations Using Quantum Mechanical Potentials*, Ph.D. Dissertation, University of Florida, 2004.
- ³¹ Y-W Hsiao, K. Runge, M. G. Cory, and R. J. Bartlett, *J. Phys. Chem. A* **105**, 704 (2001).
- ³² M. Schaible, *Critical Reviews in Solid State and Material Sciences* **24**, 265 (1999).
- ³³ D. W. Brenner D.W., *Phys. Stat. Sol (b)***217**, 23(2000).
- ³⁴ S. Tsuneyuki, M. Tsukada, H. Aoki, and Y. Matsui, *Phys. Rev. Lett.* **61**, 869 (1998).
- ³⁵ B. W. H. van Beest, G. J. Kramer, and R. A. van Santen, *Phys. Rev. Lett.* **64**, 1955 (1990).
- ³⁶ D. E. Goldberg, *Genetic Algorithms in Search, Optimization, and Machine Learning* (Addison-Wesley, New Jersey, 1989).
- ³⁷ P. Charbonneau, *Astrophysical J. Supplement Series* **101**, 309 (1995).
- ³⁸ C. Zhu, P. Byrd, Lu, J. Nocedal, Tech. Report NAM-II EFCS Department (Northwestern University, 1994).
- ³⁹ U. C. Singh and P. A. Kollman, *J. Comp. Chem.* **7**, 718 (1986).
- ⁴⁰ D. Das, K. P. Eurenus, E. M. Billings, D. C. Chatfield, M. Hodos, and B. R. Brooks, *J. Chem. Phys.*, **117**, 10534 (2002).
- ⁴¹ M. Swart, *Int. J. Quan. Chem.* **91**, 177 (2003).
- ⁴² N. Reuter, A. Dejaegere, B. Maigret, and M. Karplus, *J. Phys. Chem. A.* **104**, 1720 (2000).
- ⁴³ X. Assfeld and J. L. Rivail, *Chem. Phys. Lett.* **263**, 100 (1996).
- ⁴⁴ J. Gao, P. Amara, C. Alhambra, M. J. Field, *J. Phys. Chem.* **102**, 4714 (1998).
- ⁴⁵ J. Pu, J. Gao, and D. G. Truhlar, *J. Phys. Chem A* **108**, 632 (2004).
- ⁴⁶ I. Antes and W. Thiel, W., *J. Phys. Chem. A* **103**, 9290 (1999).
- ⁴⁷ J. Stewart in *Reviews in Computational Chemistry - Vol. 1*, (VCH Publishers, 1990).
- ⁴⁸ M. J. S. Dewar and W. Thiel, *J. Am. Chem. Soc.* **99**, 4899 (1977).
- ⁴⁹ Y. Zhang, T-S Lee, and W. Yang, *J. Chem Phys*, **110**, 46 (1999).
- ⁵⁰ F. Maseras, K. Morokuma, *J. Comp. Chem.*, **16**, 1170 (1995).
- ⁵¹ S. Humbel, S. Sieber, and K. Morokuma, *J. Chem. Phys.* **16**, 1959 (1996).

- ⁵² M. Svensson, S. Humbel, R. D. J. Froese, T. Matsubara, S. Sieber, and K. Morokuma, Phys. Chem. **100**, 19357 (1998).
- ⁵³ S. Dapprish, I. Kormaromi, K. S. Byun, K. Morokuma, M. J. Frish, J. Mol. Struct: THEOCHEM **1**, 461 (1999).
- ⁵⁴ R. Poteau, I. Ortega, F. Alary, A. R. Solis, J-C. Barthelat, and J-P. Daudey, J. Phys. Chem. **105**, 198 (2001).
- ⁵⁵ R. S. Mulliken, J. Chem. Phys. **23**, 1833 (1955).
- ⁵⁶ N. Troullier and J. L. Martins, Phys. Rev. B **43**, 1993 (1991).
- ⁵⁷ N. Troullier and J. L. Martins, Phys. Rev. B **43**, 8861 (1991).